Experimental Evidence on the Effect of Temperature on the Performance of a Lithium-Ion Battery

batteries

MDPI

Article

Experimental Evidence on the Effect of Temperature on the Performance of a Lithium-Ion Battery

Maurizio Bressan, Elena Campagnoli * and Valter Giaretto

Department of Energy, Politecnico di Torino, 24 c.so Duca degli Abruzzi, 10129 Torino, Italy; maurizio.bressan@polito.it (M.B.); valter.giaretto@polito.it (V.G.)
* Correspondence: elena.campagnoli@polito.it

Abstract

The current energy transition highlights the importance not only of energy production, but also of its efficient storage, for which lithium-ion batteries are currently the leading technology. In many applications, these devices operate outdoors at temperatures below 0 °C, and consequently, their performance is reduced due to the lower mobility of the ions. With the aim of evaluating this decrease in performance, measurements were carried out on a commercial $LiFePO_4$ module in the temperature range −20–+55 °C. The results show that the battery capacity decreases by 15% compared to the value measured at room temperature when the operating temperature drops to approximately −10 °C, and by 35% at approximately −20 °C. The paper also introduces a modified version of the Arrhenius kinetic model that allows for the analytical evaluation of the change in battery capacity as a function of temperature. The modified model proposes a quadratic dependence of the activation energy on the temperature through a temperature coefficient that for the two tested modules is equal to 8.0×10^{-5} eV/K^2 and 6.7×10^{-5} eV/K^2, respectively.

Keywords: $LiFePO_4$ battery; low temperature; ion mobility

Academic Editor: Mingtao Li

Received: 16 October 2025
Revised: 20 November 2025
Accepted: 24 November 2025
Published: 26 November 2025

Citation: Bressan, M.; Campagnoli, E.; Giaretto, V. Experimental Evidence on the Effect of Temperature on the Performance of a Lithium-Ion Battery. *Batteries* **2025**, *11*, 439. https://doi.org/10.3390/batteries11120439

1. Introduction

In recent years, attempts to find alternative energy resources to traditional fuels have further increased, both due to the limited temporal availability of the latter and the serious environmental consequences linked to their use. A clear alternative is to switch to renewable energy sources, which have the advantage of minimal environmental impact but pose the problem of managing the fact that, by their nature, they are predominantly intermittent, making the use of energy storage systems essential.

Depending on the needs for releasing the stored energy and the type of renewable energy to be converted, the storage system varies significantly [1–3]. Among potential storage technologies, batteries are of particular interest for several reasons, ranging from their relatively high energy density combined with low maintenance requirements [4,5] to the flexibility they allow for the electrical system [6]. There are many battery technologies available, but lithium-ion batteries currently represent the leading technology since they are characterized by high efficiency and relatively high energy density [7], though their impact on the environment cannot be neglected [8].

There are several types of lithium batteries on the market, the main difference between them being the chemical composition of the cathode, while the anode is usually made of graphite, regardless of the composition of the cathode. In addition to lithium, the cathode

can contain other transition metal elements such as titanium, manganese, iron, cobalt, and nickel.

Furthermore, in the case of $LiFePO_4$, some authors suggest doping the cathode with titanium, manganese, iron, cobalt, or carbon nanotubes [9–12] to increase both ion conductivity and battery performance.

The chemical composition of the cathode determines some essential characteristics of the battery, including capacity, power (maximum electrical current), performance, cost, safety, and number of charge/discharge cycles, i.e., the battery life.

Within this variety of cathodes, specific energy and power can vary greatly. For example, lithium-cobalt cathode batteries have high specific energies with not-so-high specific powers, while lithium-iron-phosphate cathode batteries have high specific powers with lower specific energies [13].

A common feature of all lithium-ion batteries is the performance degradation at extreme temperatures [14–19], particularly at low temperatures. Consequently, proper thermal management needs to be considered [15,20,21].

The paper presents, in the temperature range from -20 °C to +55 °C, the preliminary results regarding the open-circuit voltage and the so-called ohmic resistance, both of which are relevant to the charge and discharge capability of the battery module. To account for the reduction in battery performance, a kinetic model based on the classical Arrhenius model is proposed, which introduces the temperature dependence of the activation energy. The effect of localized electrical heating on improving performance at low temperatures is also evaluated.

2. Materials and Methods

Commercial lithium-iron-phosphate battery modules ($LiFePO_4$), with a solid electrolyte (e.g., polymeric- or ceramic-based) able to operate at low temperatures, were considered for the experimental investigation. According to the manufacturer (Shenzhen Zefeng Biotechnology Co., Ltd., Shenzhen, China), each module consists of a single cell with a nominal voltage of 3.2 V and nominal capacity of 23 Ah. On the contrary, no information was provided about the chemical-physical characteristics of the electrolyte and its interface with the anode and cathode. These modules have a rectangular shape, external dimensions of 150 mm × 130 mm × 15 mm, and a gross weight of 0.6 kg.

For this battery, the typical half-reactions at the cathode (the electrode where the reduction occurs) and at the anode (the electrode where the oxidation occurs) are, respectively, written as

$$LiFePO_4 \Leftrightarrow Li_{(1-x)}FePO_4 + xLi^+ + xe^-, \qquad xLi^+ + xe^- + 6C \Leftrightarrow Li_xC_6, \tag{1}$$

where both half-reactions evolving towards the right represent the charging process (anode as positive electrode), while the direction towards the left represents the discharging process (cathode as positive electrode).

Theoretically, when the battery is fully charged, there are no more available sites at the anode for Li^+ ions because it is ideally fully lithiated, and, at the same time, there is no more ionized material at the cathode because it is ideally fully delithiated. During the discharge process, at the anode and cathode, the reverse process occurs, thus completely reconstructing the $LiFePO_4$ and graphite structures.

The reactions in Equation (1) are written on a stoichiometric basis and in a perfectly reversible manner, but it is known that real operating conditions show deviations from this ideal condition.

In fact, as the battery ages, irreversible phenomena occur. Typically, these phenomena are mechanical or chemical and primarily affect the decomposition of the electrodes (e.g., the formation of dendrites on the cathode side).

When the battery is subjected to charge and discharge cycles, especially at low temperatures, its internal resistance increases, reducing both its capacity and its energy efficiency [22–24]. As a consequence of the increase in resistance, a greater increase in the battery temperature is observed, which accelerates the irreversible aging phenomena [25–27]. However, the effects of temperature alone are expected to be reversible because when the battery returns to room temperature it resumes its nominal performance.

The anode and cathode typically consist of a crystalline structure in which ions are trapped in lattice sites, while the intermediate electrolyte consists of a material that conducts ions well but not electrons. Furthermore, studies in the literature [28] demonstrate that ion migration increases in the presence of lattice defects due to the lack of proper lattice order and decreases as the temperature decreases. Moreover, it is known that for ion diffusion to occur, the lattice must contain vacancies, and the ions must have sufficient energy to pass through a vacancy. The energy required to force ions through the lattice is commonly called activation energy.

In the field of chemical kinetics of reactions, this topic is widely discussed in the literature, starting from the second half of the nineteenth century [29]. The temperature dependence of a certain equilibrium constant for a given reaction occurring at constant pressure is established by the so-called van't Hoff–Arrhenius equation, which in its original differential form can be expressed as

$$\left[\frac{\partial(lnK_C)}{\partial T}\right]_p = \frac{\Delta E}{k_B T^2}, \tag{2}$$

where K_C in this case is the dimensionless concentration constant at the equilibrium, T is the absolute temperature, and ΔE (eV) is the total amount of energy (the activation energy) for kinetics to occur, while k_B is the Boltzmann constant. By separating the variables, Equation (2) can be rewritten as

$$\frac{dK_C}{K_C} = \frac{\Delta E}{k_B T^2} dT. \tag{3}$$

In the case where the activation energy ΔE is assumed constant in the investigated temperature range, the solution of Equation (3) identifies the well-known Arrhenius equation: $\ln K_C = \ln A - (\Delta E/k_B)1/T$, where parameter A is related to the integration constant, called the pre-exponential factor, which is the intercept obtained by extrapolating $1/T \to 0$. In fact, the plot of $\ln K_C$ against $1/T$ gives a straight line with a negative slope $-(\Delta E/k_B)$. Alternatively, if for the kinetic constant we consider the reference value $K_{C,0}$ at temperature T_0 and introduce the equivalent kinetic coefficient ψ, in this case $\psi = K_C/K_{C,0}$, the solution of Equation (3) as a definite integral between T_0 and the generic temperature T is

$$\ln \psi = -\frac{\Delta E}{k_B}\left(\frac{1}{T} - \frac{1}{T_0}\right). \tag{4}$$

As established by Arrhenius, the equivalent kinetic coefficient ψ can be written in terms of the ratio of forward or backward rate constants or ionic diffusion coefficients. In general, it can be written as the ratio of any chemical quantity related to the kinetics or transport phenomenon under study. Furthermore, van't Hoff considers the possibility that the activation energy depends on a constant term, e.g., ΔE_0, and on terms both proportional to the temperature and to its square [29]. In this case, the kinetics shows a deviation from the linear trend in a semi-log plot.

In the literature, several cases can be found where this temperature dependence occurs. For example, in [30,31], where the case of ion diffusion inside the graphite anode of a lithium-ion cell is examined, the diffusion coefficient is investigated in the temperature range from −20 °C to +40 °C. In [30], in the mentioned temperature range, the ionic diffusion coefficients δ were determined every 10 K.

Figure 1 shows (empty circles) a trend of $\ln \psi$, which is clearly non-linear with respect to $1/T$. This trend was obtained by choosing as reference the measured ionic diffusion coefficient δ_0 at T_0 = 40 °C and considering $\psi = \delta/\delta_0$ and $T < T_0$. In fact, if we assume that the activation energy ΔE_0 at T_0 is constant and use Equation (4), the trend proposed by Arrhenius is indicated in Figure 1 by the dashed line. As visible in Figure 1, the slope $-\Delta E_0/k_B$ allows us to reproduce only the few values included in the first 20 K from T_0, providing an activation energy of an ion equal to $\Delta E_0 = 2.6 \times 10^{-5}$ eV.

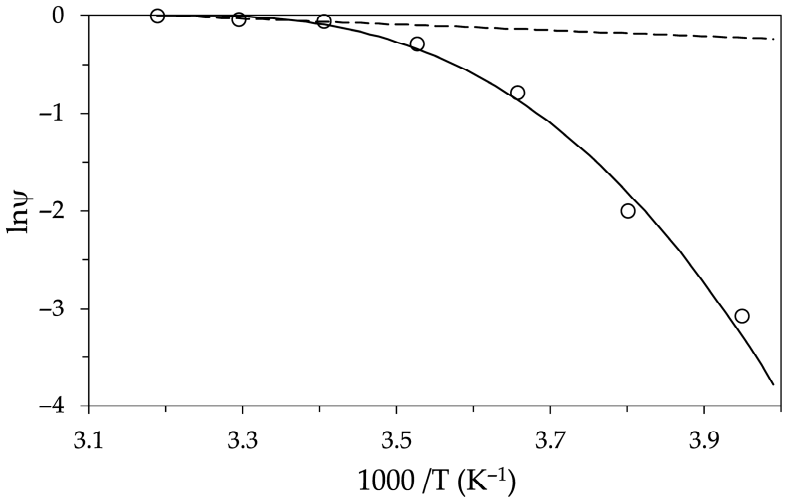

Figure 1. Semi-log diagram of the equivalent kinetic coefficient vs. the reciprocal of the absolute temperature. The empty circles refer to the measured values found in the literature [30], and the dashed and solid lines represent the solution of the classical Arrhenius equation and the modified version proposed here, respectively.

Since the trend of the measured data is non-linear over the entire temperature range, a temperature dependence for the activation energy was imposed. The temperature dependence was assigned as a deviation from ΔE_0 via a quadratic function of the temperature difference from the reference value T_0:

$$\Delta E(T) = \Delta E_0 + m(T - T_0)^2, \tag{5}$$

where m (eV/K^2) represents a proper constant temperature coefficient. Reconsidering the solution of Equation (3) with the assigned $\Delta E(T)$:

$$\frac{d\delta}{\delta} = \frac{\Delta E_0 + m(T - T_0)^2}{k_B T^2} dT = \frac{\Delta E_0 + m\left(T^2 - 2T_0 T + T_0^2\right)}{k_B T^2}. \tag{6}$$

By integrating from δ_0 to δ and from T_0 to T, with $\psi = \delta/\delta_0$ the following modified Arrhenius equation was obtained:

$$\ln \psi = -\left\{ \frac{\Delta E_0}{k_B}\left(\frac{1}{T} - \frac{1}{T_0}\right) + \frac{m}{k_B}\left[(T - T_0) + 2T_0 \ln\left(\frac{T}{T_0}\right) + T_0^2\left(\frac{1}{T} - \frac{1}{T_0}\right)\right]\right\}. \tag{7}$$

Note that Equation (6) with $m = 0$ yields the solution obtained with the classical Arrhenius model, as shown in Equation (4). If we assume the previously found value for ΔE_0, with $m = 2.76 \times 10^{-4}$ eV/K^2, we obtain the trend represented by the solid line in Figure 1, which is in good agreement with measurements over the whole temperature range.

In the case of anodic graphite, for ion diffusion to occur at low temperatures, the activation energy required increases by several orders of magnitude, as evident in Figure 1. In fact, at a temperature of 250 K, the energy required for ion mobility is approximately five times the value at T_0. Therefore, in the absence of an adequate electric gradient, as the temperature decreases the ions stop.

Although these considerations only concern data relating to the anode, it can be assumed that a similar kinetic mechanism occurs for the cathode and the electrolyte. The kinetic model proposed through Equation (7) will thus be used in the following section to describe the temperature trend of the investigated battery in equilibrium conditions. More specifically, through this kinetic we will try to justify the effect of temperature on the battery capacity, attributing this effect to the impossibility of providing the ions with the activation energy necessary for their mobility.

3. Results and Discussion

The temperature effect was investigated in the range from −20 °C to +55 °C. The maximum test temperature was chosen as the operating limit for safety reasons while the minimum temperature was assumed as a critical value related to external climatic conditions. Two modules were utilized. The first module was used to find the relationship between open-circuit voltage (OCV) and state of charge (SOC) at different operating temperatures. The second was used to study the effect of temperature on the charge and discharge capacity of the battery and to verify the ability of the modified Arrhenius kinetics of Equation (7) to reproduce the experimental trend.

Since the aim was to highlight the effects of temperature on battery performance, it was assumed that the use of a single current for the charging and discharging processes did not represent an a priori limitation and therefore all tests were performed using a current of ±11.5 A corresponding to 0.5 C.

In Figure 2, the sketch of the experimental set-up is shown.

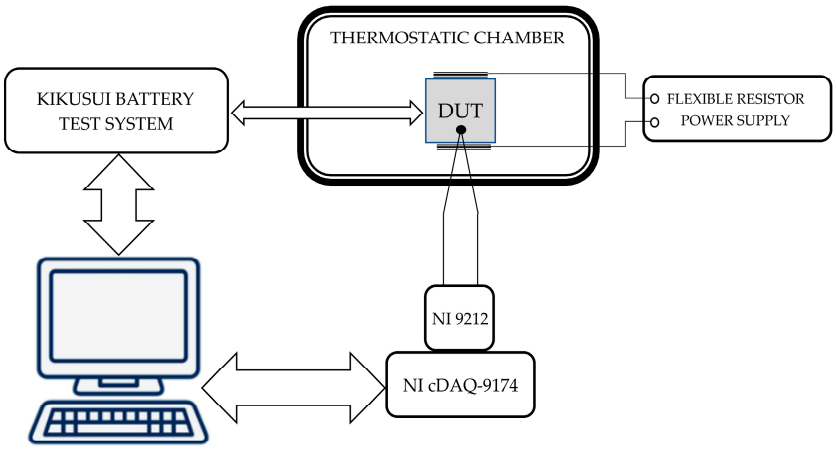

Figure 2. Schematic of the experimental set-up.

A Kikusui (Kikusui Electronics Europe GmbH, Duesseldorf, Germany) battery test system equipped with a PFX2512 charge/discharge system controller, a PWR800L DC power supply (0–40 V, 0–80 A), and a PLZ1004W electronic load was used for the tests. The manufacturer declares for this device a voltage resolution equal to 0.1 mV and a current resolution equal to 0.1 mA, with high speed and high accuracy. The controller can perform

charging and discharging processes at a constant current, constant voltage, constant power, and any user-defined current-voltage time profile.

To determine the OCV versus SOC, it was assumed that, regardless of the test temperature, the initial SOC of the battery is equal to the maximum achievable SOC at room temperature, which is therefore assumed to be 100% of the SOC. To limit any damage to the battery caused by overvoltage, the maximum charging voltage was set to V_{MAX} = 3.55 V, i.e., approximately 110% of the nominal voltage. The battery was then fully charged in two phases. The first phase was at a constant current (+11.5 A). This phase, which can last from a few minutes to several hours depending on the initial charge level, stops when the V_{MAX} is reached. The second phase was at constant voltage (V_{MAX}), with a maximum duration of 1.5 h, which was considered sufficient time to reach a supply current close to zero. Then, to determine the actual OCV when the SOC is 100%, a relaxation time of 1.5 h was imposed, during which the control system is at rest (zero supply current).

Figure 3 shows, as an example, the current and voltage trend as a function of time for the room temperature test. The figure shows how the voltage decays during the relaxation period toward an asymptotic value. Some authors [32] assume the calculated value of this asymptote as the actual OCV value.

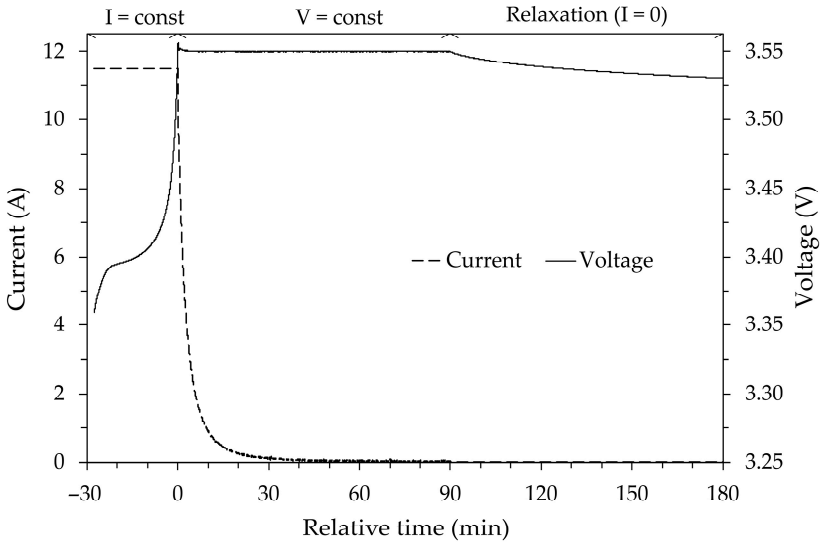

Figure 3. Current (I) and voltage (V) profiles for charging at room temperature. Negative relative time values refer to the constant current phase.

In the tests performed, it was assumed that at the end of the imposed relaxation time (1.5 h) the measured voltage is very close to its asymptotic value and therefore practically coincident with the actual OCV.

During the discharge phase, the minimum voltage value at which the battery is considered completely discharged (0% SOC) was set to approximately 85% of the nominal voltage, i.e., V_{MIN} = 2.7 V. This choice is due to both the potential damage to the battery when the voltage values reached during the discharge phase are excessively low and, where applicable, the need to maintain a battery voltage high enough to guarantee an adequate supply voltage for the loads connected to it. Regardless of these reasons, it has been found that below the V_{MIN} voltage, the energy that the battery can still supply is practically negligible.

A rest/relaxation time of 1.5 h was also set for the discharge phase, which begins when V_{MIN} is reached and at the end of which the measured voltage value corresponds to the OCV.

Since the battery was assigned a SOC of 100% after charging at room temperature, the minimum SOC, which depends on the actual energy released during discharge and

is expected to vary with temperature, was not set to zero at the end of all discharge tests. To identify the actual battery capacity at room temperature, several complete charge and discharge cycles were performed at constant current (±11.5 A) in the chosen operating voltage range. Using simply constant current Coulomb counting, the capacity of the battery was evaluated during discharge, measuring the time needed to reach V_{MIN} from the OCV measured at 100% SOC, and during charge by measuring the time needed to reach V_{MAX} from the OCV measured at the end of the previous discharge. Under these conditions, the actual battery capacity at room temperature was, on average, slightly lower than the nominal capacity, and the maximum value found, equal to 21.8 Ah, was chosen as a reference value, C_{REF}, to determine the SOC level at the different test temperatures.

Both the battery charging and discharging were carried out in steps designed to vary the nominal battery capacity (23 Ah) by 5% each time. Using a constant charge/discharge current of ±11.5 A, the duration of each stage was 6 min, followed by a relaxation time of 1.5 h, after which the OCV was assigned. An example is shown in Figure 4 for the initial discharging phase. The current and voltage graphs are plotted as a function of relative time, which refers to the end of the relaxation time of the previous charging procedure (SOC 100%), which showed an OCV equal to 3.53 V. In the figure, the dashed line represents the current values, while the solid line represents the voltage measured at the battery terminals. The voltage curve over time is, as expected, exponential with a horizontal asymptote. It can be noted that the first discharge step (fully charged battery) has a greater voltage drop than the following step. This behavior is, as is known, linked to the so-called activation losses which cause the reaction to initially occur more slowly. It can also be observed that, during the relaxation period between the two discharges shown in the figure, the voltage increases by a few hundredths of a volt.

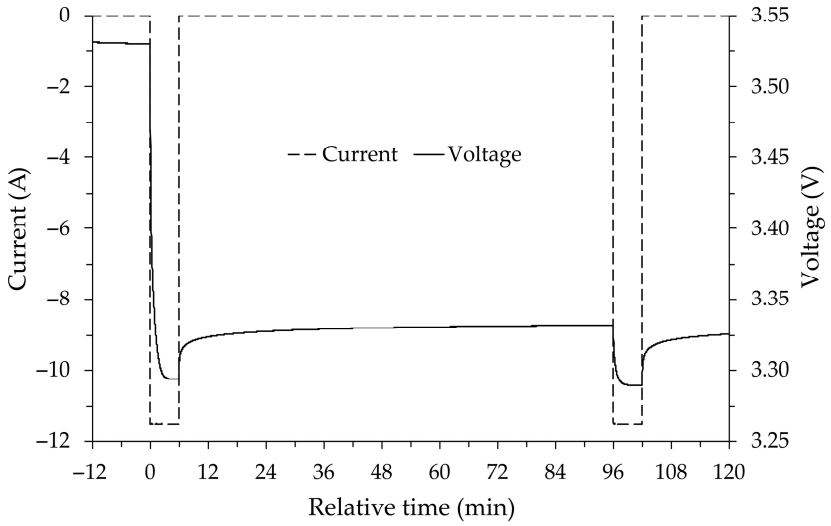

Figure 4. Current and voltage as a function of relative time for the initial part of the discharge phase at room temperature. Negative values of the relative time refer to the relaxation period of the previous charging procedure.

After the initial voltage drop due to activation, the various discharge phases occur regularly and a gradual decrease in the OCV is observed, which remains above the nominal voltage even at low SOC values. The final part of the discharge process is shown in Figure 5, where at relative time zero, the battery state of charge is approximately 10.1%.

In Figure 5, the discharge starting at relative time zero still occurs regularly, but it is observed that the voltage curve over time has a negative concavity with an apparently vertical asymptote in the final part of the discharge phase. This voltage behavior already begins to manifest when the SOC value drops below 30%, but when the SOC reaches 10%,

the voltage shows a much sharper drop. As can be seen in Figure 5, this sharp voltage reduction causes the voltage to drop below V_{MIN} during the next discharge, so that the control system shuts down the load after only a couple of minutes. If the load is reapplied, the energy exchanged in the subsequent steps is minimal and at the end of the test the SOC is approximately 1.5% and the OCV is equal to 2.82 V.

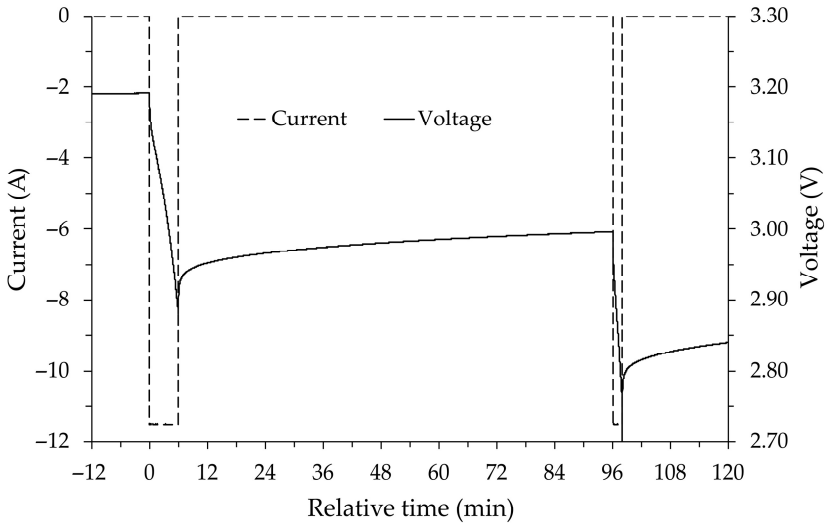

Figure 5. Current and voltage vs. relative time in the final part of discharging at room temperature. Negative values for the relative time refer to the relaxation period at SOC 10.1%.

Figure 6, which has the same relative time equal to zero as Figure 5, shows the temperature trend of the device over time, measured on the external surface of the battery, during the different discharge steps. The comparison between the two figures highlights how a sudden decrease in voltage corresponds to a sudden increase in temperature. Figure 6 shows that for negative values of the relative time, the temperature trend is almost regular, increasing during the application of the current load and decreasing during the relaxation phase, returning to approximately the initial value. On the positive side of the time axis, a sudden increase in temperature can be observed, albeit by a few tenths of a degree, which certainly indicates a singular event within the battery, likely an increase in internal resistance, the thermal effect of which disappears in the following step when the load duration decreases. While these calorimetric aspects could provide interesting insights into the electrochemical behavior of the battery, they are beyond the scope of this work.

Starting from the SOC and OCV values obtained after the discharge sequence, the charging procedure was performed again using constant current steps corresponding to 5% of the nominal capacity. As shown in Figures 7 and 8, the behavior of the battery during charging is similar to that observed during discharging, and therefore similar considerations can be drawn. During charging, the thermal behavior of the battery is comparable to that found during discharging, even with regard to the final part of the charge, highlighting a temperature trend similar to that shown in Figure 6. For this test performed at room temperature, the reference temperature of the device was calculated as the average of the temperatures during the discharge and charge phases and is approximately 22.0 °C.

The set of OCV against SOC values determined at room temperature during the discharge and charge are shown in Figure 9. In the figure, the circles and triangles represent the values measured during the charging and discharging steps, respectively, and the error bars for the voltage are equal to 1%. Observing the trends for the two phases, the voltage values are almost superimposable within the error bar. Therefore, it is not possible to highlight significantly different behaviors of the battery during discharge and charge at room temperature. The presence of hysteresis in the discharge and charge cycle is

predictable, since a difference in OCV during charge and discharge has always been found for the same SOC.

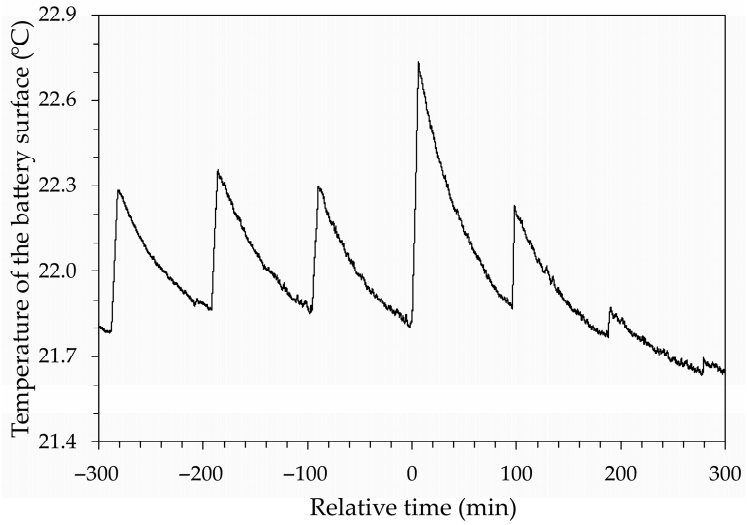

Figure 6. Temperature vs. time for the final part of the discharging process. Relative time zero is the same as shown in Figure 5.

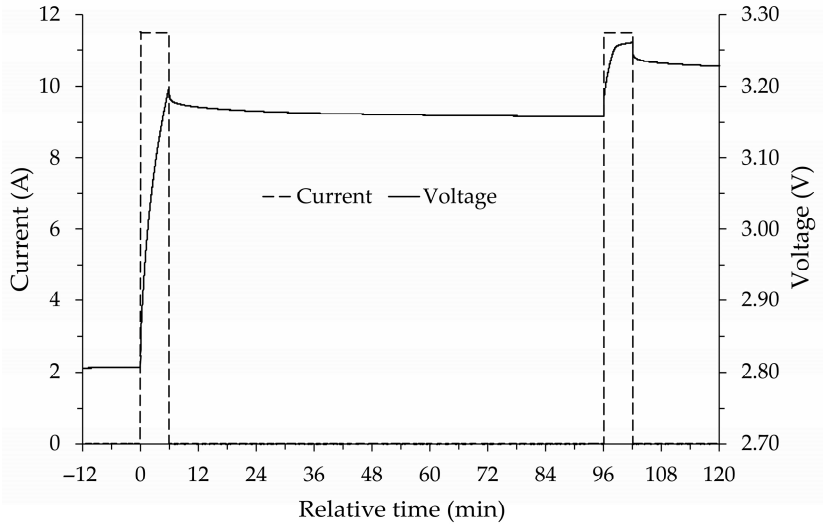

Figure 7. Current and voltage vs. time for the initial part of charging at room temperature. Negative values for the relative time refer to the end of the relaxation period after the discharge.

The solid line shown in Figure 9 represents the trend of OCV as a function of SOC calculated using a model available in the literature [33] which reports the following equation:

$$OCV = a + b \cdot [-\ln(SOC)]^p + c \cdot SOC + d \cdot exp[q \cdot (SOC - 1)]; \;\; 0 < SOC \leq 1 \qquad (8)$$

where in the case of a $LiFePO_4$ battery operating at room temperature, the parameter values are as follows: $a = 3.135\ V$, $b = -0.685\ V$, $c = -1.342\ V$, $d = 1.734\ V$, $p = 0.478$, $q = 0.4$.

As can be seen, when the SOC varies from approximately zero up to 90%, the model shows OCV values in good agreement with the measured ones. On the contrary, when the SOC exceeds 90%, the model is unable to fit the measured values since the voltage is approximately constant when approaching 100% SOC. Tests at temperatures other than room temperature were carried out in a thermostatic chamber by sequentially selecting one of the following set points: 0 °C, −10 °C, −20 °C, and finally +55 °C.

Before each of these tests, to ensure the same initial conditions, the battery, following the procedure described above, was fully charged (100% SOC) at room temperature. After

obtaining a stable temperature in the chamber, the various 5% discharge and charge steps were performed using a current of ±11.5 A. The exchanged energy and the resulting capacity change at each step were determined by Coulomb counting, calculating the SOC level using the previously-determined C_{REF} value as a reference capacity.

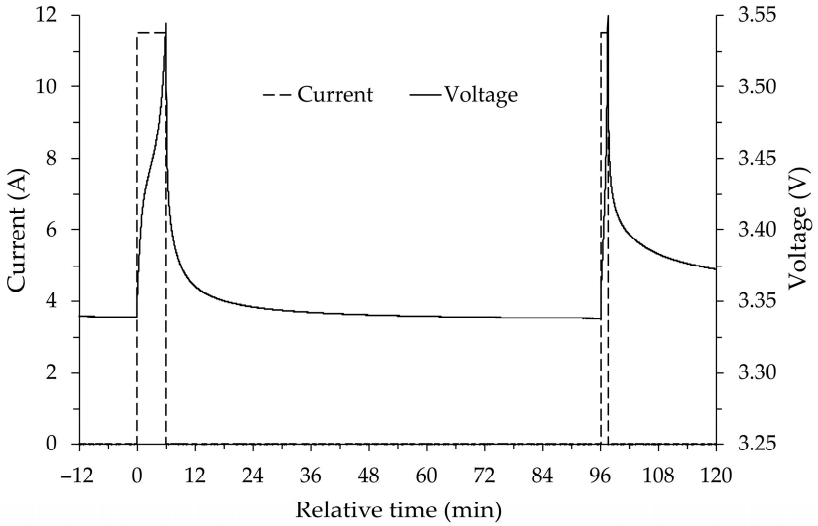

Figure 8. Current and voltage vs. time for the final part of charging at room temperature. Negative values for the relative time refer to the relaxation period at SOC 92.9%.

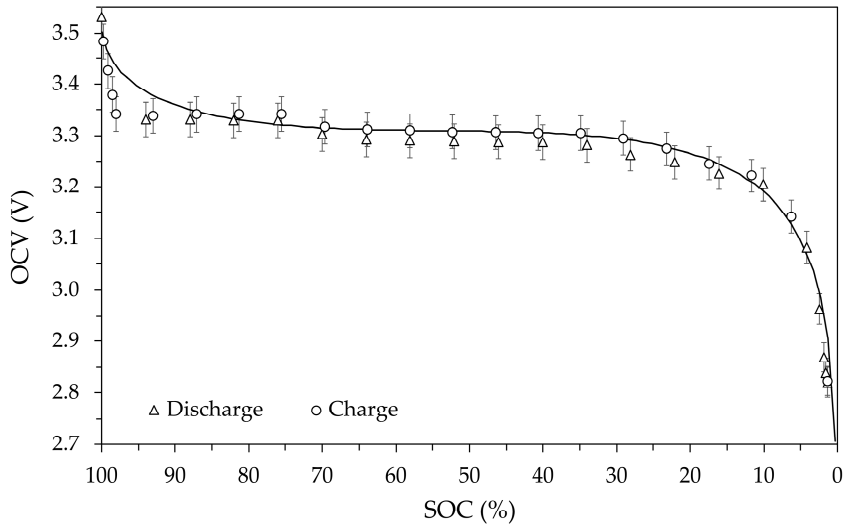

Figure 9. Open-circuit voltage vs. state of charge at the calculated average battery temperature of 22.0 °C. Error bars are 1%.

The OCV-measured values as a function of SOC for the different temperatures are shown in Figures 10 and 11 for the discharge and charge process, respectively. As shown in the figures, the average temperature values measured on the external surface of the battery are 22.0 °C, 2.0 °C, −9.1 °C, −19.7 °C, and 52.2 °C. Furthermore, in the figures, the theoretical model OCV vs. SOC at room temperature is shown (solid line).

Looking at Figure 10, it can be observed that when the SOC is above 35%, the OCV values are practically independent of temperature and have deviations of less than 2%. Furthermore, in this range, the theoretical model approximates the experimental data with a deviation of no more than 2%.

Figure 10 also shows that at temperatures below 0 °C, battery performance in terms of both voltage level and available energy is significantly reduced compared to at room

temperature. Indeed, at the test temperatures of −9.1 °C and −19.7 °C, a significant reduction in available battery capacity of approximately 15% and 35%, respectively, as well as an overall reduction in OCV, can be observed.

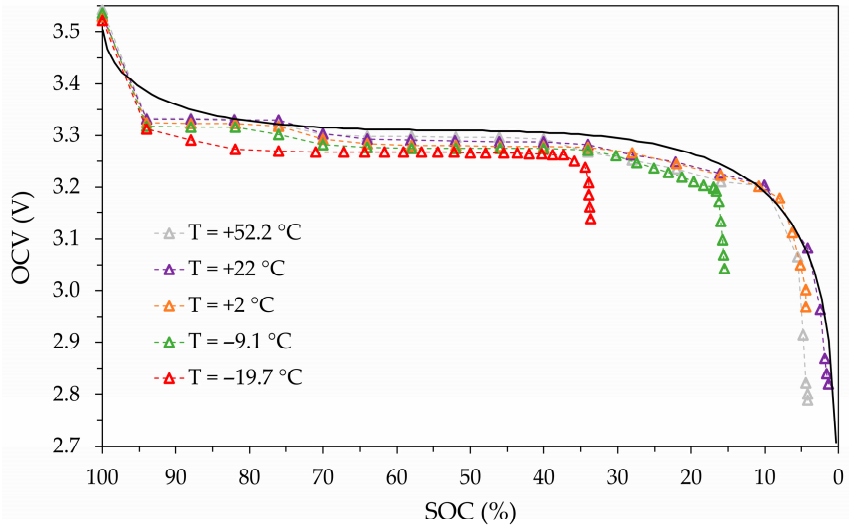

Figure 10. OCV vs. SOC at different battery temperatures during the discharge process. The continuous line represents the theoretical model (Equation (8)) at room temperature.

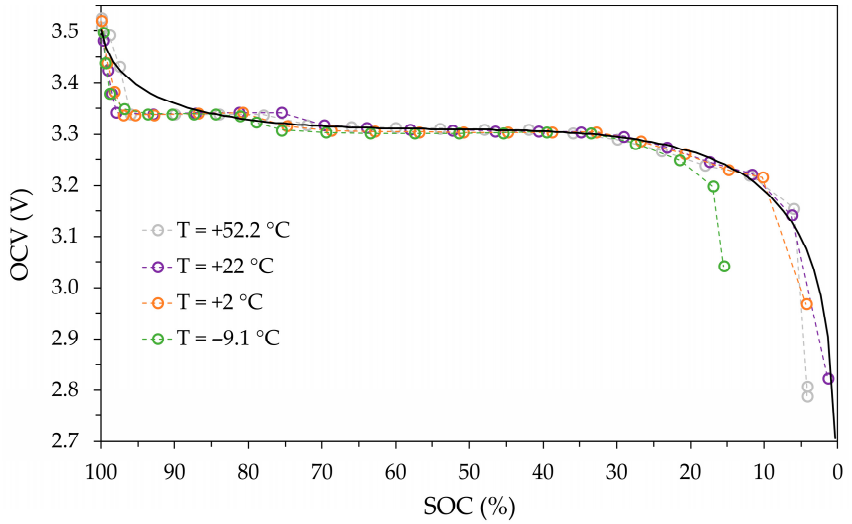

Figure 11. OCV vs. SOC at different battery temperatures during the charge process. The continuous line represents the theoretical model (Equation (8)) at room temperature.

Figure 11 shows that for the charging process, for SOC values between 25% and 90%, the OCV values are virtually independent of temperature, and the theoretical model fits the experimental data very well. For SOC values above 90%, it can be observed that the model is no longer able to reproduce the experimental data, which are still independent of temperature.

Figure 11 does not show the test performed at the nominal temperature of −20 °C because it was not possible to charge the battery at this temperature. The cause of this "failure" could be the electrolyte, the characteristics of which are unknown since the only information provided by the manufacturer refers to the nominal voltage and capacity values. Indeed, as reported in the literature [34], it can be assumed that since solid electrolytes already at room temperature exhibit substantial interfacial resistances and low ionic conductivities, this aspect becomes even more relevant at low temperatures. The reduction in ion mobility at low temperatures makes ion migration paths less accessible

and consequently requires a higher activation energy for diffusion to occur. In the case of the tests presented in this paper, at a temperature close to −20 °C, the required activation energy is so high that ion conduction stops due to the overvoltage limit. It is worth noting that this temperature-induced limitation appears reversible. Indeed, it has been found that by returning the battery to room temperature, the OCV shown in Figure 9 is practically reproducible without apparent irreversibility or definitive losses of capacity.

These critical issues disappear at temperatures above 0 °C. In fact, observing the curves at +2.0 °C and +52.2 °C, it can be noted that, apart from a reduction of approximately 5% in the useful capacity in both cases, the OCV vs. SOC trends are similar and comparable with the test at room temperature.

The OCV values measured at the end of the discharge processes increase as the battery temperature decreases (Figure 10). For example, at a temperature of approximately −20 °C, the OCV was found to be close to 3.15 V, while at a temperature of about +52 °C, the measured voltage was just above 2.75 V. Since the change in the molar Gibbs free energy Δg (J/mol) due to both half-reactions reported in Equation (1) is proportional to the OCV, in standard conditions it can be written as

$$\Delta g = -n \cdot F \cdot OCV, \tag{9}$$

where F is the Faraday constant (C/mol) and n is unitary in this case.

Figure 12 shows the molar Gibbs free energy obtained using the OCV values measured at the end of discharge at the different temperatures. The dashed line represents the linear regression performed on these values, and the error bars refer to a 2% deviation. In the same temperature range, it is interesting to note that the temperature dependence of the molar Gibbs free energy of a $LiFePO_4$ reported in the literature is also linear [35] and shows the same slope as the regression line in Figure 11, even though the literature values refer only to the cathode material.

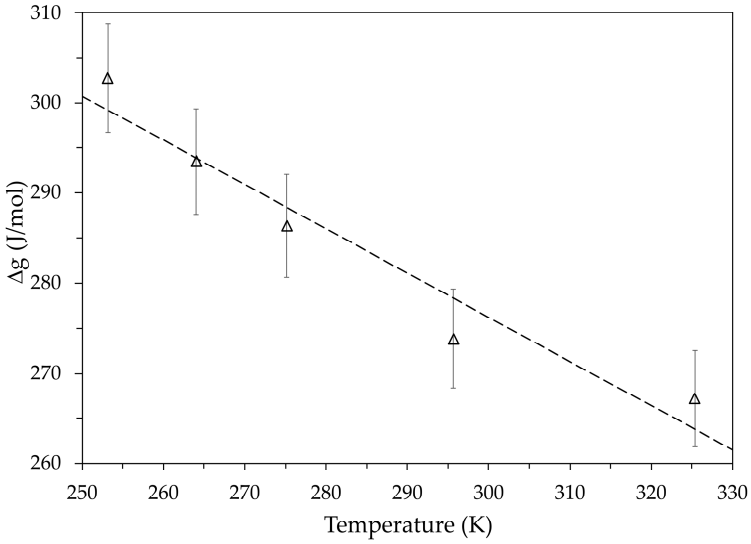

Figure 12. Molar Gibbs free energy vs. temperature. Triangles are the values obtained measuring the OCV at the end of discharge. Error bars represent 2% deviation, and dashed line is the linear regression of the measured values.

The reduced ionic mobility thus appears to actually cause a decrease in battery capacity, which is particularly noticeable at temperatures below 0 °C. Despite this criticality, as mentioned above, experimental tests have shown that increasing the battery temperature can restore its capacity to a value close to the nominal one. Since this occurs in tests aimed

at finding a relationship between OCV and SOC, to further investigate this behavior, a new set of measurements was performed using a second new module.

The new battery was initially charged, discharged, and recharged at room temperature following the procedure described above. The new reference value for its capacity is C_{REF} = 22.4 Ah. The tests were carried out in the thermostatic chamber with a fixed set point of −20 °C. In these new tests, to increase the temperature of the battery relative to that of the chamber, a square-shaped film heating resistor (40 mm × 40 mm) capable of providing a heat flux in the range 0–48 W was applied to each of the two large external surfaces of the battery.

The tests were performed using the previous voltage limits (V_{MAX} = 3.55 V and V_{MIN} = 2.7 V) and the same constant current (±11.5 A). The battery was first subjected to a continuous discharge (V_{MIN} voltage reached) followed by a relaxation time of 1.5 h, and then a continuous charge (V_{MAX} voltage reached).

Comparing these continuous discharge and charge processes with those performed in steps, it was noted that in this case the heat generation due to the Joule effect produces higher internal temperatures in the battery than those previously measured. Despite this, the relaxation period between discharge and charge is sufficient for the temperature to return to the value before discharge, allowing discharge and charge to be carried out under similar thermal conditions (the same average temperature).

With the thermostatic chamber set to −20 °C, several discharge/charge cycles were performed, during which the resistors were powered by progressively increasing the thermal power used to heat the battery. For each test, the change in battery capacity was measured at the temperature reached with the help of the resistors. The results obtained show that, for both the discharging and charging processes, the battery capacity decreases as its temperature decreases, in line with what was seen using the previous battery. It is important to note that with this second module, it was possible to carry out both the discharge and charge processes down to a minimum temperature of −17.3 °C without the aid of a heating resistor. Comparing this result with that obtained with the previous battery, which could not be charged at −19.7 °C, suggests that the threshold temperature that inhibits ionic conduction in the electrolyte falls within this narrow temperature range.

The set of results obtained for the two batteries was interpreted using the modified Arrhenius model proposed in Equation (7). Since the kinetic parameter ψ can be related to the ionic mobility and the consequent change in battery capacity, it has been established that ψ is equivalent to the ratio C_T/C_{REF}, where C_T corresponds to the battery capacity measured at a given temperature, while C_{REF} represents its value at room temperature.

The results are summarized in the semi-logarithmic diagram of Figure 13 for both battery modules. In this figure, the dashed line (module #1) and solid line (module #2) represent the output of the kinetic model of Equation (7). The model assumed the same value for the activation energy, $\Delta E_0 = 1.0 \times 10^{-3}$ eV, and different values for the temperature coefficient, $m = 8.0 \times 10^{-5}$ eV/K^2 for module #1, and $m = 6.7 \times 10^{-5}$ eV/K^2 for module #2. The need for a higher temperature coefficient for the first module is likely due to its level of thermal aging. Indeed, the first module was subjected to numerous charge and discharge cycles and a much higher number of test hours (several hundred) than the second. Looking at the graph, it can be observed that, even considering measurement uncertainties of 5% for both tests, the different temperature behavior remains.

The good agreement between the proposed model and the measurements seems to confirm the possibility of expressing the performance of a battery using a kinetic approach in which the reduced ionic mobility is considered by assuming that the activation energy is a function of temperature. Furthermore, based on experimental data, it is possible to state

that the battery capacity depends only on its thermal level and not on the discharge/charge process performed.

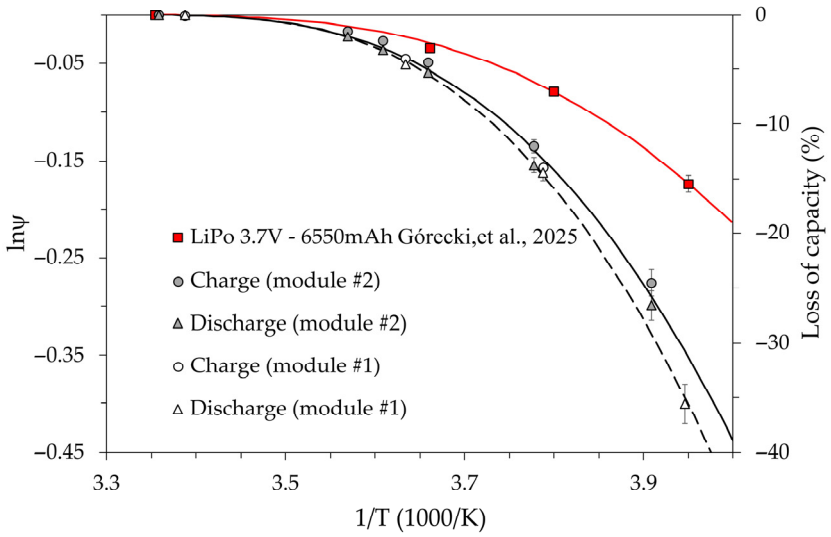

Figure 13. Semi-log diagram of the equivalent kinetic coefficient vs. the reciprocal of the absolute temperature. The black dashed (module #1) and solid (module #2) lines for the $LiFePO_4$, and the red solid line for the LiPo [36] refer to the modified Arrhenius model proposed in Equation (7). Error bars are 5%.

Figure 13 also shows on the right vertical axis the absolute value of the percentage capacity loss evaluated with respect to the reference value C_{REF}. In this figure, it is possible to note that at the same temperature, the capacity loss during charging is always lower than that found during discharging. Although the difference is generally small (less than 5%), it cannot be explained by the kinetic model, which depends only on temperature.

Figure 13 also reports the data available in the literature [36] relating to the reduction in capacity at low temperatures for a LiPo battery. Even in the case of this different type of battery, the modified Arrhenius model seems to be able to reproduce the trend of the measured data with a good level of accuracy (error bars 5%). Also, for this battery, the activation energy at the reference temperature is assumed equal to $\Delta E_0 = 1.0 \times 10^{-3}$ eV, while the temperature coefficient is in this case $m = 3.3 \times 10^{-5}$ eV/K^2.

Since charging or discharging times depend on the instant at which the voltage extreme V_{MIN} and V_{MAX} are reached, the electrical resistance of the electrodes can also be relevant. In equivalent electrical circuits used to simulate the dynamic behavior of a battery, the ohmic resistance R_0 is associated with the instantaneous drop or increase in voltage when the current is interrupted or allowed to flow in the battery, respectively.

Figure 14 shows the ohmic resistance versus temperature determined for module #2 at the beginning of the discharge and charge. The temperature dependence of R_0 is highly non-linear, both during discharge and charge. It is difficult to attribute this behavior only to the material of electrodes, and we cannot exclude the possibility that it is due to a peculiar characteristic of the specific battery assembly. Even assuming a 10% uncertainty in determining the resistance R_0, the value found for discharging was always higher than that for charging. This could justify the greater battery capacity achieved during charging compared to that available during discharging at the same temperature and could also explain the lower OCV value observed during discharging compared to charging.

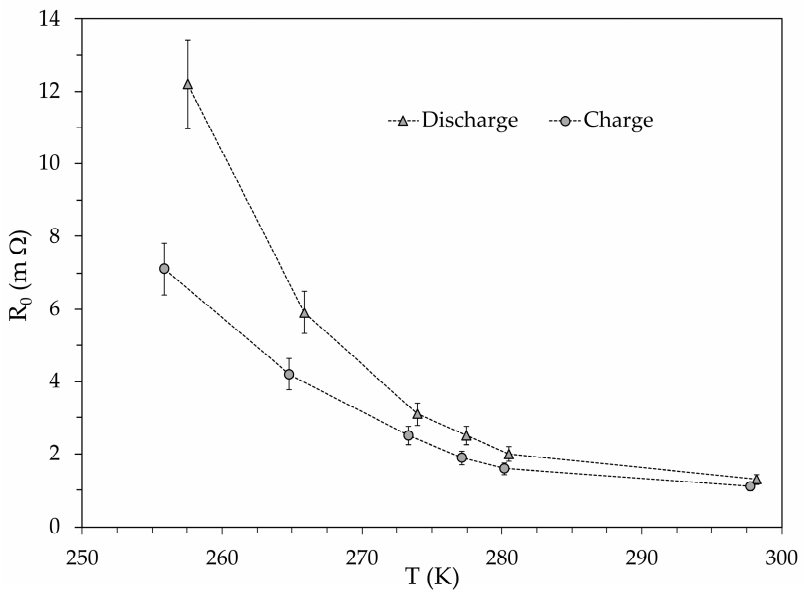

Figure 14. Diagram of ohmic resistance for the discharge and charge vs. absolute temperature for battery module #2. Error bars are 10%.

4. Conclusions

A preliminary experimental investigation of the thermal behavior of a lithium-iron-phosphate battery was proposed. The main objective of the experiment was to verify the possibility of using a kinetic model to determine the reduction in battery capacity as the operating temperature decreases. Some concluding remarks are highlighted as follows:

- The relationship found between OCV and SOC is in good agreement with models proposed in the literature. This allows us to consider the chosen battery as representative of the lithium-iron-phosphate type.
- The reduction in battery capacity as the temperature decreases appears to be mainly attributable to ion conduction of electrolytes. Decreasing the temperature gradually makes the migration paths of ions within its structure less accessible. Therefore, for each type of electrolyte, there may be a threshold temperature that inhibits ionic conduction.
- The reduction in battery capacity due to low temperatures appears reversible. In fact, returning the battery to higher temperatures restores the expected capacity value.
- Electron conduction also appears to influence battery performance at low temperatures. Experimental results show a significant increase in the so-called ohmic resistance at temperatures below ambient.

The results presented for $LiFePO_4$ must be considered preliminary and have some limitations. These include the unknown chemical and physical properties of the electrolyte and the limited test conditions implemented, which involve a single charge and discharge current and short cycling. In addition, the reference temperatures for the tests are only local measurements performed on both of the large surfaces of the thin battery. In the case of a battery with a different geometry, the temperatures measured on the surface could be less representative. For these reasons, the authors believe it would be useful and interesting to continue the research by performing tests at different temperatures and charge/discharge currents, increasing the number of cycles, and extending the investigation to other types of lithium batteries. Furthermore, for a better thermal characterization of the battery, suitable thermal models should be implemented.

Author Contributions: Conceptualization, M.B., E.C. and V.G.; methodology, V.G.; investigation, M.B., E.C. and V.G.; writing—original draft preparation, E.C. and V.G.; writing—review and editing, E.C. and V.G. All authors have read and agreed to the published version of the manuscript.

Funding: This research received no external funding.

Data Availability Statement: The raw data supporting the conclusions of this article will be made available by the authors on request.

Conflicts of Interest: The authors declare no conflicts of interest.

Abbreviations

The following abbreviations are used in this manuscript:

OCV	Open-Circuit Voltage
SOC	State of Charge

References

1. Sayed, E.T.; Olabi, A.G.; Alami, A.H.; Radwan, A.; Mdallal, A.; Rezk, A.; Abdelkareem, A.M. Renewable Energy and Energy Storage Systems. *Energies* **2023**, *16*, 1415. [CrossRef]
2. Koohi-Fayegh, S.; Rosen, M.A. A review of energy storage types, applications and recent developments. *J. Energy Storage* **2020**, *27*, 101047. [CrossRef]
3. Detka, K.; Górecki, K. Selected technologies of electrochemical energy storage—A review. *Energies* **2023**, *16*, 5034. [CrossRef]
4. Lamnatou, C.; Chemisana, D.; Cristofari, C. Smart grids and smart technologies in relation to photovoltaics, storage systems, buildings and the environment. *Renew. Energy* **2022**, *185*, 1376–1391. [CrossRef]
5. Pimm, A.J.; Cockerill, T.T.; Taylor, P.G. The potential for peak shaving on low voltage distribution networks using electricity storage. *J. Energy Storage* **2018**, *16*, 231–242. [CrossRef]
6. Impram, S.; Nese, S.V.; Oral, B. Challenges of renewable energy penetration on power system flexibility: A survey. *Energy Strateg. Rev.* **2020**, *31*, 100539. [CrossRef]
7. Chen, T.; Jin, J.; Lv, H.; Yang, A.; Liu, M.; Chen, B.; Xie, Y.; Chen, Q. Applications of Lithium-Ion Batteries in Grid-Scale Energy Storage Systems. *Trans. Tianjin Univ.* **2020**, *26*, 208–217. [CrossRef]
8. Bawankar, S.; Dwivedi, G.; Nanda, I.; Jimenez Macedo, V.D.; Kesharvani, S.; Meshram, K.; Jain, S.; Mishra, S.; Singh, V.P.; Verma, P. Environmental impact assessment of lithium-ion battery employing cradle to grave. *Sustain. Energy Technol. Assess.* **2023**, *60*, 103530. [CrossRef]
9. Akhmetova, K.; Sultanov, F.; Mentbayeva, A.; Umirov, N.; Bakenov, Z.; Tatykayev, B. Advances in multi-element doping of $LiFePO_4$ cathode material for capacity enhancement in Li-ion batteries. *J. Power Sources* **2024**, *624*, 235531. [CrossRef]
10. Zhang, F.; Huang, J.; Zong, F.; Tuo, K.; Cai, X.; Zhou, X.; Zhao, D.; Cui, X.; Li, S.; Zhang, N. Effect of Ti content on preparation of $LiFePO_4$ cathode from $FeSO_4{\cdot}7H_2O$ waste residue. *J. Alloys Compd.* **2023**, *955*, 170270. [CrossRef]
11. Abdelaal, M.M.; Alkhedher, M. Dual optimization of $LiFePO_4$ cathode performance using manganese substitution and a hybrid lithiated Nafion-modified PEDOT:PSS coating layer for lithium-ion batteries. *Electrochim. Acta* **2024**, *506*, 145050. [CrossRef]
12. Al-Samet, M.A.M.M.; Burgaz, E. Improving the lithium-ion diffusion and electrical conductivity of $LiFePO_4$ cathode material by doping magnesium and multi-walled carbon nanotubes. *J. Alloys Compd.* **2023**, *947*, 169680. [CrossRef]
13. Miao, Y.; Hynan, P.; von Jouanne, A.; Yokochi, A. Current Li-Ion Battery Technologies in Electric Vehicles and Opportunities for Advancements. *Energies* **2019**, *12*, 1074. [CrossRef]
14. Liao, L.; Zuo, P.; Ma, Y.; Chena, X.; Ana, Y.; Gaoa, Y.; Yin, G. Effects of temperature on charge/discharge behaviors of $LiFePO_4$ cathode for Li-ion batteries. *Electrochim. Acta* **2012**, *60*, 69–273. [CrossRef]
15. Jin, G.; Zhao, W.; Zhang, J.; Liang, W.; Chen, M.; Xu, R. High-Temperature Stability of $LiFePO_4$/Carbon Lithium-Ion Batteries: Challenges and Strategies. *Sustain. Chem.* **2025**, *6*, 7. [CrossRef]
16. Issa, F.; Diaconu, E.M.; Ardeleanu, M.N. Working temperature's influence on the $LiFePO_4$ battery generated power. *Sci. Bull. Electr. Eng. Fac.* **2023**, *2*, 1–4. [CrossRef]
17. Gong, X.; Mi, C.C. Temperature-dependent performance of lithium-ion batteries in electric vehicles. In Proceedings of the 2015 IEEE Applied Power Electronics Conference and Exposition (APEC), Charlotte, NC, USA, 15–19 March 2015; pp. 1065–1072. [CrossRef]
18. Alipour, M.; Ziebert, C.; Conte, F.V.; Kizilel, R. A Review on Temperature-Dependent Electrochemical Properties, Aging, and Performance of Lithium-Ion Cells. *Batteries* **2020**, *6*, 35. [CrossRef]

19. Karlsen, H.; Dong, T.; Yang, Z.; Carvalho, R. Temperature-Dependence in Battery Management Systems for Electric Vehicles: Challenges, Criteria, and Solutions. *IEEE Access* **2019**, *7*, 142203–142213. [CrossRef]
20. Azizi, Y.; Sadrameli, S.M. Thermal management of a $LiFePO_4$ battery pack at high temperature environment using a composite of phase change materials and aluminum wire mesh plates. *Energy Conv. Manag.* **2016**, *128*, 294–302. [CrossRef]
21. Zhou, L.; Garg, A.; Li, W.; Gao, L. Intelligent temperature control framework of lithium-ion battery for electric vehicles. *Appl. Therm. Eng.* **2024**, *236 Pt C*, 121577. [CrossRef]
22. Zhang, Q.; White, R.E. Capacity fade analysis of a lithium-ion cell. *J. Power Sources* **2008**, *179*, 793–798. [CrossRef]
23. Jaguemont, J.; Boulon, L.; Dubé, Y. A comprehensive review of lithium-ion batteries used in hybrid and electric vehicles at cold temperatures. *Appl. Energy* **2016**, *164*, 99–114. [CrossRef]
24. Singer, J.P.; Birke, K.P. Kinetic study of low temperature capacity fading in Li-ion cells. *J. Energy Storage* **2017**, *13*, 129–136. [CrossRef]
25. Rauhala, T.; Jalkanen, K.; Romann, T.; Lust, E.; Omar, N.; Kallio, T. Low-temperature aging mechanisms of commercial graphite/$LiFePO_4$ cells cycled with a simulated electric vehicle load profile—A post-mortem study. *J. Energy Storage* **2018**, *20*, 344–356. [CrossRef]
26. Omar, N.; Abdel Monem, M.; Firouz, Y.; Salminen, J.; Smekens, J.; Hegazy, O.; Gaulous, H.; Mulder, G.; Van den Bossche, P.; Coosemans, T.; et al. Lithium iron phosphate-based battery–Assessment of the aging parameters and development of cycle life model. *Appl. Energy* **2014**, *113*, 1575–1585. [CrossRef]
27. Zhang, G.; Wei, X.; Han, G.; Dai, H.; Zhu, J.; Wang, X.; Tang, X.; Ye, J. Lithium plating on the anode for lithium-ion batteries during long-term low temperature cycling. *J. Power Sources* **2021**, *484*, 229312. [CrossRef]
28. Sotoudeh, M.; Baumgart, S.; Dillenz, M.; Döhn, J.; Forster-Tonigold, K.; Helmbrecht, K.; Stottmeister, D.; Groß, A. Ion Mobility in Crystalline Battery Materials. *Adv. Energy Mater.* **2024**, *14*, 2302550. [CrossRef]
29. Laidler, K.J. The Development of the Arrhenius Equation. *J. Chem. Educ.* **1984**, *61*, 494–498. [CrossRef]
30. Zhang, S.S.; Xu, K.; Jow, T.R. Low temperature performance of graphite electrode in Li-ion cells. *Electrochim. Acta* **2002**, *48*, 241–246. [CrossRef]
31. Yang, H.; Wu, N. Ionic conductivity and ion transport mechanisms of solid-state lithium-ion battery electrolytes: A review. *Energy Sci. Eng.* **2022**, *10*, 1643–1671. [CrossRef]
32. Theuerkauf, D.; Swan, L. Characteristics of Open Circuit Voltage Relaxation in Lithium-Ion Batteries for the Purpose of State of Charge and State of Health Analysis. *Batteries* **2022**, *8*, 77. [CrossRef]
33. Zhang, C.; Jiang, J.; Zhang, L.; Liu, S.; Wang, L.; Loh, P.C. A generalized SOC-OCV model for lithium-ion batteries and the SOC estimation for LNMCO battery. *Energies* **2016**, *9*, 900. [CrossRef]
34. Shanbedi, M.; Shahali, H.; Polycarpou, A.A.; Amiri, A. Advances and future prospects of low-temperature electrolytes for lithium-ion batteries. *EEE Batteries* **2025**, *1*, 385–426. [CrossRef]
35. Wang, S.; Zhang, G.; Gao, J.; Wang, J.; Wang, Y.; Nan, C.; Huang, D.; Chen, L.; Song, J.; Luo, P. First-principles Study on $LiFePO_4$ Materials for Lithium-ion Battery. In Proceedings of the International Workshop on Materials, Chemistry and Engineering (IWMCE 2018), Xiamen, China, 16–17 June 2018; pp. 133–138.
36. Górecki, K.; Ptak, P. SPICE-Aided modeling characteristics of selected batteries. *Energies* **2025**, *18*, 4709. [CrossRef]